Nonlinear model predictive control of organic Rankine cycles for automotive waste heat recovery: Is it worth the effort?

Yannic Vaupel[a], Jan C. Schulze[a], Adel Mhamdi[a], Alexander Mitsos[b,a,c,*]

[a] *RWTH Aachen University, AVT - Aachener Verfahrenstechnik, Process Systems Engineering, Forckenbeckstraße 51, D - 52074 Aachen*
[b] *JARA Energy*
[c] *Institute of Energy and Climate Research - Energy Systems Engineering (IEK-10), Forschungszentrum Jülich GmbH, Wilhelm-Johnen-Straße, 52425 Jülich, Germany*

Abstract

Using organic Rankine cycles (ORC) for waste heat recovery in vehicles promises significant reductions in fuel consumption. Controlling the organic Rankine cycle, however, is difficult due to the highly transient exhaust gas conditions. To tackle this issue, nonlinear model predictive control (NMPC) has been proposed and approximate NMPC solutions have been investigated to reduce computational demand. Herein, we compare (i) an idealized economic NMPC (eNMPC) scheme as a benchmark to (ii) a NMPC enforcing minimal superheat and (iii) a PI controller with dynamic feed-forward term (PI-ff) in a control case study with highly transient disturbances. We show that, for an ORC system with supersonic turbine, the economic control problem can be reduced to a single-input single-output superheat tracking problem combined with a decoupled steady-state real-time optimization (RTO) of turbine operation, assuming an idealized condenser. Our results indicate that the NMPC enforcing minimal superheat provides good control performance with negligible losses in average power compared to the full solution of the economic NMPC problem and that even PI-ff only results in marginal losses in average power compared to the model-based controllers.

*Corresponding author: A. Mitsos
Email address: amitsos@alum.mit.edu (Alexander Mitsos)

Keywords: advanced model-based control, dynamic optimization, minimal superheat, feed-forward control

1. Introduction

In order to reduce fuel consumption of vehicles, waste heat recovery (WHR) is considered a promising approach [1, 2]. Among the available technologies for WHR, employing a bottoming organic Rankine cycle (ORC) has been widely investigated. The technology has been primarily proposed for heavy-duty vehicles as economic feasibility appears achievable [3], though publications for passenger vehicles exist [4–7]. Among the potential heat sources, the exhaust gas and exhaust gas recirculation are typically preferred over the coolant as the associated fluid streams exhibit higher exergy flow rates [8].

ORC operation in vehicles results in challenges, which are not encountered in traditional fields of ORC application. Constraints regarding economics and available space mandate that the system has to be cheap, lightweight and relatively small. Furthermore, the control system has to operate the ORC system safely and efficiently under extreme heat source fluctuations with limited computational power available. The former point is addressed in a wide range of publications considering cycle optimization [9, 10], working fluid selection [11], working fluid design [12, 13] and expander optimization. The reader is referred to [14] for a recent review.

Control of ORC systems for vehicles is addressed in many publications. The proposed methods range from classical PID-type controllers [15] including feed-forward term [16, 17], linear model predictive control (LMPC) with single [18, 19] or multiple models [20, 21], dynamic programming [22], to nonlinear model predictive control (NMPC) with regulatory objective [23] and economic NMPC (eNMPC) [24, 25]. NMPC is associated with high control quality, but also with high computational cost, making on-board implementation question-

able. In eNMPC, a nonlinear model predictive control problem with an objective function motivated by process economics is solved [26]. Fast NMPC methods that approximate the NMPC solution have been applied to WHR in vehicles and real-time capability was reported on desktop computers [27, 28]. For an overview of this class of control algorithms we refer to [29]. Furthermore, ANN-based NMPC [30] and explicit NMPC [31] have been proposed to address the high computational demand of NMPC.

Recent works also compare advanced model-based controllers to PI controllers [27, 28, 32]. In [27], a real-time iteration (RTI) scheme [33] is implemented with ACADO [34] for a parallel heat exchanger WHR system. The NMPC scheme is found to result in a significantly higher net power production (about 9 %) than PID-based control, which is predominantly due to the latter failing to meet the superheat constraint resulting in the turbine being bypassed. In [28], a RTI scheme with economic objective including moving horizon estimation is implemented for a single heat exchanger system and compared to a PID controller and a LQR. The authors find that the eNMPC scheme only improves power production by about 2 % compared to the other controllers. In [32], three different advanced control strategies are compared for a system with a single heat exchanger. While NMPC with tracking objective and dynamic programming with economic objective yield similar net power production, a PID-based strategy results in significantly lower net power production. This is predominantly due to intermediate bypassing of the turbine as the superheat constraint is not satisfied at all times.

While many control-related contributions focusing on the development and performance evaluation of particular controllers are available, comparatively few publications address what constitutes optimal operation/control for the considered ORC system. Answering this question requires considerations on (i) what are the control objectives and (ii) which degrees of freedom should be employed to control the system. These points are addressed to some extent in [35, 36] and

[37]. We recently presented a manuscript that uses dynamic optimization to find optimal operating policies for characteristic operating scenarios [38]. There, we compared operation at minimal superheat to optimal economic operation with flexible superheat. For a scenario, where no operational constraints besides minimal superheat become active, we found that economically optimal system operation included several peaks in superheat similar to those in the fuzzy logic strategy in [37]. However, as the additional produced power is small, we proposed to operate at minimal superheat. Further, we found, in line with [35], that working fluid (WF) mass flow should be the main actuator and the evaporator bypass should only be used to satisfy operational constraints. This can for example be necessary when, temporarily, only a limited amount of recovered power can be utilized. In this situation, we found that operating at increased superheat can improve overall power production. Our findings indicate that it is crucial to consider the system dynamics for optimal operation and stress the need for energy management approaches, as e.g., [39].

In this manuscript, we transfer our findings to a control strategy. We implement a NMPC scheme based on single shooting which solves each instance of the optimal control problem (OCP) to convergence. Using this scheme, we develop (i) a controller with economic objective function and (ii) a controller with regulatory objective function. For comparison, we implement (iii) a PI controller with feed-forward term. Subsequently, we test the controllers in-silico with an ORC model from our previous work [38, 40] on a driving cycle with highly transient disturbances. The aforementioned contributions that include comparisons between advanced model-based controllers and PI controllers [27, 28, 32] focus on developing real-time capable advanced control strategies. In contrast, our focus is on discussing different approaches to the control problem and assessing the limit of the economic benefit of NMPC over decentralized control strategies under idealized assumptions. We show that (i) the multi-variable control problem can be addressed by a decentralized control structure without significant loss of performance assuming an ideal condenser and (ii) employing a PI controller

with feed-forward term leads only to small losses in produced power compared to NMPC.

In the case study, we assume that the power produced can be fully utilized at all times. Note that irrespective of whether the expansion machine is mechanically coupled to the powertrain or connected to a generator, situations may occur, where the amount of power that can be utilized is limited. Such a situation would require an energy management system that switches to a different operating regime (as outlined in [38]) and is not considered herein.

The remainder of this manuscript is structured as follows. We introduce our modeling assumptions and the process model in Sec. 2 followed by a presentation of the examined control strategies in Sec. 3. We present a case study based on the World Harmonized Transient Cycle (WHTC) in Sec. 4 and present conclusions in Sec. 5.

2. Investigated system

We consider an ORC process for waste heat recovery in a heavy-duty diesel truck (Fig. 1). The liquid working fluid (WF) ethanol is pressurized in a pump ④→①, evaporated at high pressure in the evaporator ①→②, expanded in the turbine ②→③ and liquefied in the condenser ③→④. The heat source is the tailpipe exhaust gas with mass flow rate $\dot{m}_{exh}$ and inlet temperature $T_{exh,in}$. We only consider the high-pressure side and assume an ideal condenser with constant WF outlet conditions as is common practice in control literature [35]. The ORC model is taken from our previous work [40] with the simplifications introduced in [38]. The turbine is modeled using a quasi-stationary model and the evaporator is modeled with the moving boundary approach [41]. The available inputs for manipulating the system are the WF mass flow rate $\dot{m}_{WF,in}$ set by the pump, the turbine rotational speed n_{turb} and the exhaust gas bypass valve position x_{BPV}. As the turbine operates at supersonic conditions, n_{turb} does not

affect the WF outlet mass flow from the evaporator [35]. Thus, it only serves as degree of freedom to optimize turbine operation [38]. Our findings from [38] indicate that, for a typical driving cycle, the exhaust gas bypass valve position can be fixed so that all exhaust gas passes through the evaporator and power production is maximized. Consequently, we do not consider x_{BPV} as a degree of freedom (DOF) in this work. The disturbances are $\dot{m}_{exh}$ and $T_{exh,in}$. We only consider nominal operation, i.e., the fluid enters the evaporator as subcooled liquid and exits as superheated vapor. Thus, we do not require a switching model as developed in [42].

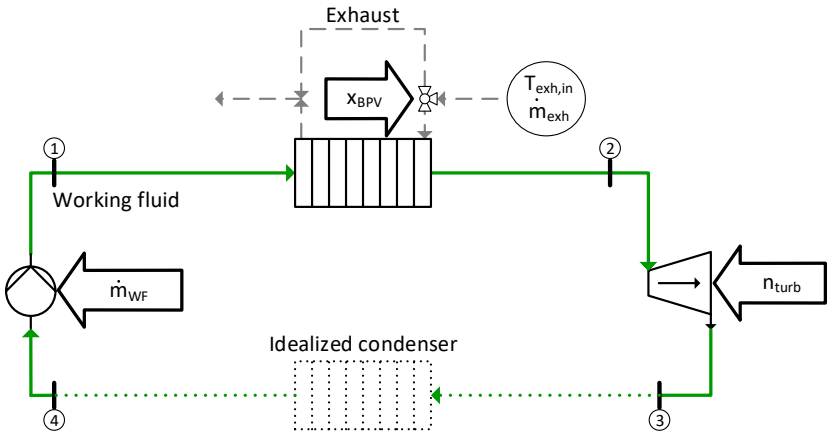

Figure 1: Topology of the examined system (taken from [38]). The WF is indicated by the solid green line and the exhaust gas by the dashed gray line. The control variables are indicated by arrows and the disturbances by the circle. The condenser is replaced by the idealized assumption of operation at ambient pressure and fixed subcooling.

3. Examined control strategies

In this section, we first discuss the control objectives, the DOF considered for controlling the system and we describe the considered control structures based on our findings in [38] (Sec. 3.1). Then, we present (i) the eNMPC, (ii) the NMPC (both in Sec. 3.2) and (iii) PI controller with feed-forward term (PI-ff) in Sec. 3.3.

3.1. Considered control structures, objectives and degrees of freedom

The ultimate objective of a WHR system in a vehicle is to reduce fuel consumption. Assuming that the produced power can always be fully utilized, the control objective is to maximize produced electric power while achieving safe operation by manipulating the considered DOF ($\dot{m}_{WF,in}$, n_{turb}). For eNMPC, we can directly formulate the economic objective function accordingly and for all MPC controllers, we have to determine adequate constraints. Herein, we refer to control structures, where not all DOF are controlled by one controller as decentralized control structures. To translate the objective of maximizing power production into a decentralized control structure, we need to pair controlled variables with the DOF and specify adequate set-points.

A variety of decentralized control structures has been suggested in literature and distinction has to be drawn between ORC system with volumetric expanders, where the expander speed influences the WF mass flow rate [43] and supersonic turbines, where this is not the case [35]. For volumetric expanders, it is proposed to use pump mass flow to control superheat and expander speed to control evaporating temperature [16]. For turbines, using pump mass flow to control superheat is a sensible choice [35]. The control structure can be extended by using the exhaust bypass to additionally control pressure [36]. This additional control loop could be used by an energy management system to adjust the power output. In works with MPC, authors either choose a regulatory objective function that minimizes the deviation from a superheat set-point [27] or a desired WF temperature [23] (NMPC) or an economic objective function [25, 28] which maximizes net power production (eNMPC).

We assess the differences between MPC formulations with (i) economic objective function (eNMPC) and (ii) regulatory objective function (NMPC), with turbine operation being optimized separately in the latter case. Furthermore, we implement (iii) a PI controller with feed-forward term that tracks a constant superheat set-point and uses the same turbine optimization procedure as (ii).

3.2. Nonlinear model predictive control (NMPC)

NMPC relies on a repeated solution of an OCP on a finite horizon. The system dynamics are explicitly considered through a model and constraints can be imposed on state and input trajectories. Feedback is introduced by initializing the dynamic problem with the current system state, implementing only part of the solution and re-solving the problem to account for disturbances and plant-model mismatch. We solve the following OCP

$$\min_{\boldsymbol{u},s} \quad \int_{t_0^{OCP}}^{t_f^{OCP}} L\left(\boldsymbol{x}\left(t\right),\boldsymbol{y}\left(t\right),\boldsymbol{u}\left(t\right)\right) + \rho_{T_{sup}} s\left(t\right)\,\mathrm{d}t \tag{1}$$

$$\text{s.t.} \quad \dot{\boldsymbol{x}}\left(t\right) = \boldsymbol{f}\left(\boldsymbol{x}\left(t\right),\boldsymbol{y}\left(t\right),\boldsymbol{u}\left(t\right),\boldsymbol{d}\left(t\right)\right) \qquad \forall t \in \left[t_0^{OCP}, t_f^{OCP}\right] \tag{2}$$

$$\mathbf{0} = \boldsymbol{g}\left(\boldsymbol{x}\left(t\right),\boldsymbol{y}\left(t\right),\boldsymbol{u}\left(t\right),\boldsymbol{d}\left(t\right)\right) \qquad \forall t \in \left[t_0^{OCP}, t_f^{OCP}\right] \tag{3}$$

$$\boldsymbol{x}\left(t_0^{OCP}\right) = \boldsymbol{x}_0 \tag{4}$$

$$\boldsymbol{h}\left(\boldsymbol{x}\left(t\right),\boldsymbol{y}\left(t\right),\boldsymbol{u}\left(t\right),\boldsymbol{d}\left(t\right)\right) \leqslant \mathbf{0} \qquad \forall t \in \left[t_0^{OCP}, t_f^{OCP}\right] \tag{5}$$

$$\boldsymbol{u}^{min} \leqslant \boldsymbol{u}\left(t\right) \leqslant \boldsymbol{u}^{max} \qquad \forall t \in \left[t_0^{OCP}, t_f^{OCP}\right] \tag{6}$$

$$\Delta T_{sup}^{min} - \Delta T_{sup}\left(t\right) - s\left(t\right) \leqslant 0 \qquad \forall t \in \left[t_0^{OCP}, t_f^{OCP}\right] \tag{7}$$

$$0 \leqslant s\left(t\right) \qquad \forall t \in \left[t_0^{OCP}, t_f^{OCP}\right] \tag{8}$$

on a horizon from initial time t_0^{OCP} to final time t_f^{OCP}. The objective function (1) is of Lagrange-type with running cost function L. The running cost functions for eNMPC and NMPC are presented in Sec. 3.2.1 and Sec. 3.2.2, respectively. The differential and algebraic equations are described by vector-valued functions $\boldsymbol{f}$ and $\boldsymbol{g}$, where $\boldsymbol{x}$ are the differential states, $\boldsymbol{y}$ are the algebraic variables, $\boldsymbol{u}$ are the controls and $\boldsymbol{d}$ are the disturbances. The inequality path constraints are described by the vector-valued function $\boldsymbol{h}$. For WF superheat, we employ a soft constraint (7) by introducing a non-negative slack variable s and adding a L1 penalty, weighted by $\rho_{T_{sup}}$, in the objective. In this work, the path constraints are enforced at the control grid points. The DOF are box-constrained in (6). The horizon is divided into N_P control intervals of length Δt_C with $t_f^{OCP} = t_0^{OCP} + N_P \Delta t_C$. The optimizer can change the DOF for the

first N_C intervals after which they are held constant. The DOF are discretized as continuous piece-wise linear functions in open-loop optimization. Note that this does allow for discontinuities of the controlled variables in closed loop. After a solution is found, the control signal is sent to the process and the problem is re-solved after one sampling interval Δt_S with t_0^{OCP} and t_f^{OCP} shifted by Δt_S.

We solve the optimal control problems with the open-source tool DyOS [44] using single shooting and warm-start the algorithm with the optimal solution from the previous time step. The integrator is NIXE [45] and the optimizer is SNOPT [46]. Since we aim to show that similar control performance as with NMPC can be achieved using simpler methods, we use full state feedback for specifying the initial state $\boldsymbol{x}_0$ in (4), as it provides an upper bound on NMPC performance. The application of state estimation to an ORC system is shown in [27] with an unscented Kalman filter, in [32] with an extended Kalman filter and in [28] with moving horizon estimation. We determine the slack penalty weights based on the Lagrange multipliers of the hard constrained problem [47].

3.2.1. Economic NMPC

Assuming that the power produced by the turbine can be fully utilized, optimal economic operation is equivalent to maximizing net power output. Thus we set $L(t) := -\left(P_{turb}(t) - P_{pump}(t)\right)$ in (1) for eNMPC. The controller adjusts $\dot{m}_{WF,in}$ and n_{turb} simultaneously. A schematic control structure is provided in Fig. 2.

3.2.2. Standard NMPC

In order to obtain good economic performance from NMPC, we have to choose a suitable controlled variable. Following ideas from self-optimizing control [48], we use the NMPC to force the process to operate at an active constraint. We design the NMPC to enforce minimal superheat, i.e., we set $L(t) := \left(\Delta T_{sup}(t) - \Delta T_{sup}^{min}\right)^2$ in (1) as it is typically the active constraint in economically optimal operation [38]. Controlling the superheat constraint is convenient,

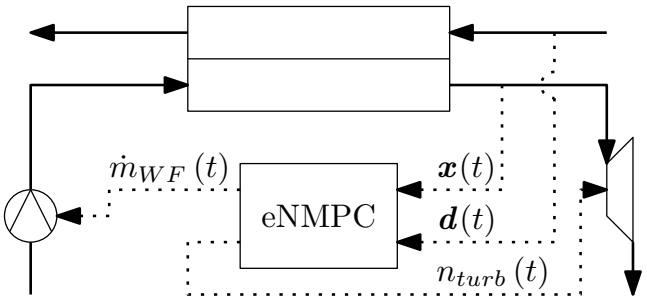

Figure 2: Control structure for eNMPC. Dotted lines indicate measurement and control signals.

as the set-point is independent of the operating conditions as opposed to, e.g., tracking an optimal pressure trajectory, but still leads to inherently optimal operation. For this objective, NMPC uses only $\dot{m}_{WF,in}$ as DOF.

Since the turbine rotational speed does not affect the WF conditions at the evaporator outlet, the objective function does not exhibit a sensitivity with respect to n_{turb}. Consequently, we determine n_{turb} in an online steady-state optimization, solved at each sampling instance of the NMPC, using `fmincon` in Matlab to optimize turbine performance. Although, the problem is non-convex, we use a local solver to maintain comparability to eNMPC where also a local solver is used. Thereby, we reduce the control problem to a single-output problem in contrast to many publications in literature where two quantities out of $T_{WF,out}$, ΔT_{sup} and p are controlled. Splitting the two optimizations is possible as the turbine rotational speed only serves to optimize turbine operation [35], which is typical for turbine expansion, but cannot be generalized to any expansion machine. A schematic representation of the control structure is provided in Fig. 3.

3.2.3. Operating constraints

In the considered case study, the pressure p^*, the WF evaporator outlet temperature $T^*_{WF,evap,out}$ and the evaporator superheat ΔT_{sup} are path constrained. Throughout this manuscript, the asterisk used as a superscript indi-

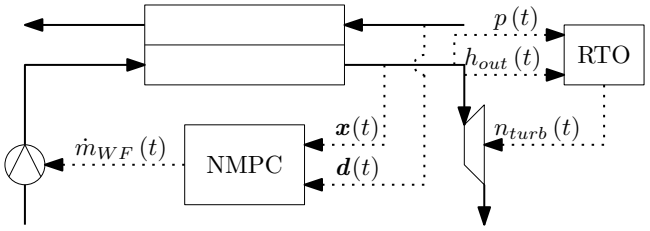

Figure 3: Control structure for NMPC. Dotted lines indicate measurement and control signals.

cates quantities that were scaled due to confidentiality reasons. Consequently, these quantities are dimensionless. The lower bound on p^* reflects the minimal pressure ratio of the turbine. Since we assume condenser operation at ambient pressure, we can directly express this as a function of the high pressure. The upper bound on p^* is a safety constraint, the upper bound on $T^*_{WF,evap,out}$ prevents WF degradation and the lower bound on ΔT_{sup} prevents damage to the turbine by droplet formation. We formulate the path constraint for ΔT_{sup} as a soft constraint and the constraints for $T^*_{WF,evap,out}$ and p^* as hard constraints. We implement the soft constraint since, in contrast to the dynamic optimization case study in [38], no prediction of the disturbances is available in this work. We expect that, as a consequence, it will not be possible to satisfy the constraint at all times. The lower and upper bounds for the path constraints and the input constraints are listed in Tab. 1. Our choice of the lower bound

Path constraints				DOF			
Variable	Unit	LB	UB	Variable	Unit	LB	UB
ΔT_{sup}	K	20	-	$\dot{m}^*_{WF,in}$	-	0.0073	0.0363
$T^*_{WF,evap,out}$	-	-	0.8719	n^*_{turb}	-	0.82	1.09
p^*	-	0.3	1.5				

Table 1: Bounds of path constraints and DOF.

of ΔT_{sup} is more conservative than in our previous publication [38], due to the unknown exhaust gas conditions in a control setting. The rationale is to provide additional back-off so that the controllers are able to maintain superheat above the limit of 10 K defined in [38]. The lower and upper bounds on $\dot{m}^*_{WF,in}$ and

n^*_{turb} represent the limits in which the model was validated [40].

3.3. PI with feed-forward term (PI-ff)

We use a PI controller with feed-forward term to track a superheat set-point using the WF mass flow as DOF

$$\dot{m}_{WF,in}(t) = K_P \cdot e(t) + K_I \int_{t_0}^{t} e(t)\,\mathrm{d}t + \dot{m}_{WF,ff}(t)\ , \tag{9}$$

where $e(t) = \Delta T^{set}_{sup} - \Delta T_{sup}(t)$ is the control error, t_0 indicates the initial time of the simulation and $\dot{m}_{WF,ff}$ is the feed-forward term. Since we want the feed-forward term to account for the dynamic response of the system, it tracks the optimal steady-state input $\dot{m}^{opt}_{WF,ss}$ according to the following differential equation

$$\dot{m}_{WF,ff}(t) + \tau_{ff}\frac{\mathrm{d}\dot{m}_{WF,ff}}{\mathrm{d}t} = \dot{m}^{opt}_{WF,ss} + \tau_z\frac{\mathrm{d}\dot{m}^{opt}_{WF,ss}}{\mathrm{d}t}\,, \tag{10}$$

where τ_{ff} and τ_z are time constants, which can be tuned to obtain a suitable dynamic behavior of the feed-forward term. Accordingly, in offset-free steady-state operation the PI-ff control action is $\dot{m}_{WF,in} = \dot{m}^{opt}_{WF,ss}$. Note that also the rate of change of the disturbances is considered on the right hand side of (10). This feed-forward policy is in accordance with [32], where the exhaust gas temperature rate of change was found to be an important input in the dynamic programming strategy.

We provide the optimal steady-state input as a map $\dot{m}^{opt}_{WF,ss} = f_{map}(\dot{m}_{exh}, T_{exh,in})$ which we determine by solving steady-state optimizations with varying heat source conditions offline and fitting the correlation with a polynomial cubic in $\dot{m}_{exh}$ and linear in $T_{exh,in}$ (Fig. 4). Similar to NMPC, PI-ff controls the WF mass flow rate only. We determine n_{turb} in a separate online steady-state optimization to obtain optimal turbine operation. A schematic representation of the PI-ff control structure is provided in Fig. 5.

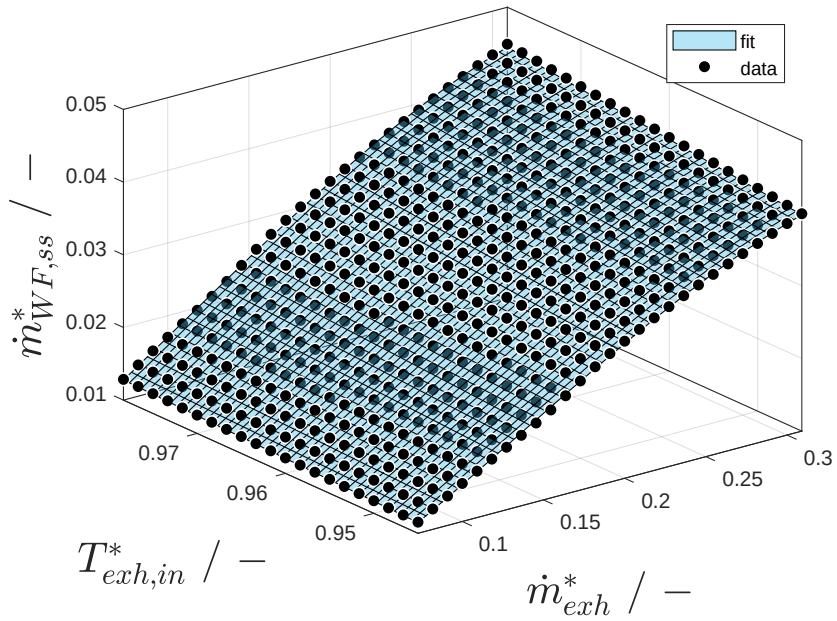

Figure 4: Polynomial fit of optimal steady-state WF flowrate as function of disturbances. The data points were obtained by steady-state optimization.

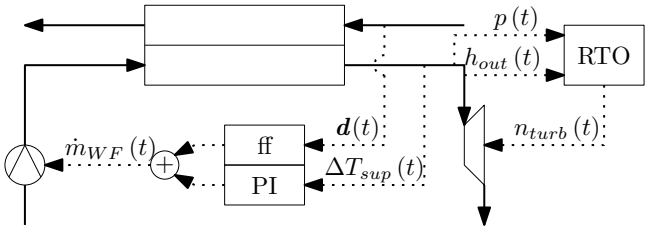

Figure 5: Control structure for PI-ff. Dotted lines indicate measurement and control signals.

4. Case study

4.1. Exhaust gas data

In this case study, we consider exhaust gas data representative of a driving cycle (Fig. 6). It was recorded on a test rig, contains parts of the World Harmonized Transient Cycle and was used in [40] for model validation and in [38] as a dynamic optimization case study. The disturbance values and their time derivatives are measured at every controller sampling instant but no prediction of the disturbances is available. The same exhaust gas mass flow and tempera-

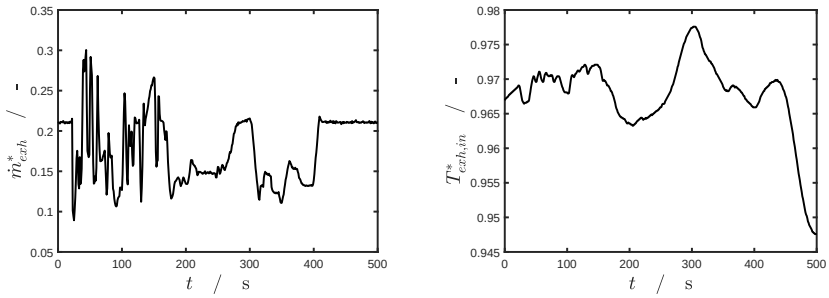

(a) Exhaust gas mass flow

(b) Exhaust gas temperature

Figure 6: Exhaust gas data for the case study.

ture data is used with all three controllers. We assume no feedback delay and no plant-model mismatch, i.e., we use the presented ORC system model for the controller and as a plant surrogate, to obtain an upper bound on NMPC performance.

4.2. Tuning of the controllers

Tuning parameters for the controllers are presented in Tab. 2. For NMPC,

	Parameter	Value	
PI-ff	K_P	-8.64×10^{-4} kg K^{-1} s^{-1}	
	K_I	1.65×10^{-6} kg K^{-1} s^{-2}	
	τ_{ff}	12.0 s	
	τ_z	1.35 s	
	ΔT^{set}_{sup}	20 K	
NMPC		economic	tracking
	N_P	5	5
	N_C	5	5
	Δt_C	8 s	8 s
	Δt_S	1 s	1 s
	$\rho_{T_{sup}}$	8 kW K^{-1}	75 K
	ΔT^{set}_{sup}	-	20 K

Table 2: Parameters for NMPC and PI-ff controller used in the case study.

we determined N_P and Δt_C by implementing various combinations and choosing the parameters that gave a feasible solution at the smallest computational cost

(i.e., small N_P at given Δt_C). We set $N_P = N_C$ as is commonly done in nonlinear model predictive control [49].

We tuned PI-ff using dynamic optimization with the objective of minimizing the squared deviation from the superheat set-point and the same exhaust gas data as in the test cycle. To validate the control law, we used data from another cycle and found PI-ff to work well. We choose $\Delta T_{sup}^{set} = 20$ K in accordance with the lower bound specified in Sec. 3.2.3.

4.3. Simulation results

The results for eNMPC, NMPC and the PI-ff are presented in Fig. 7. As

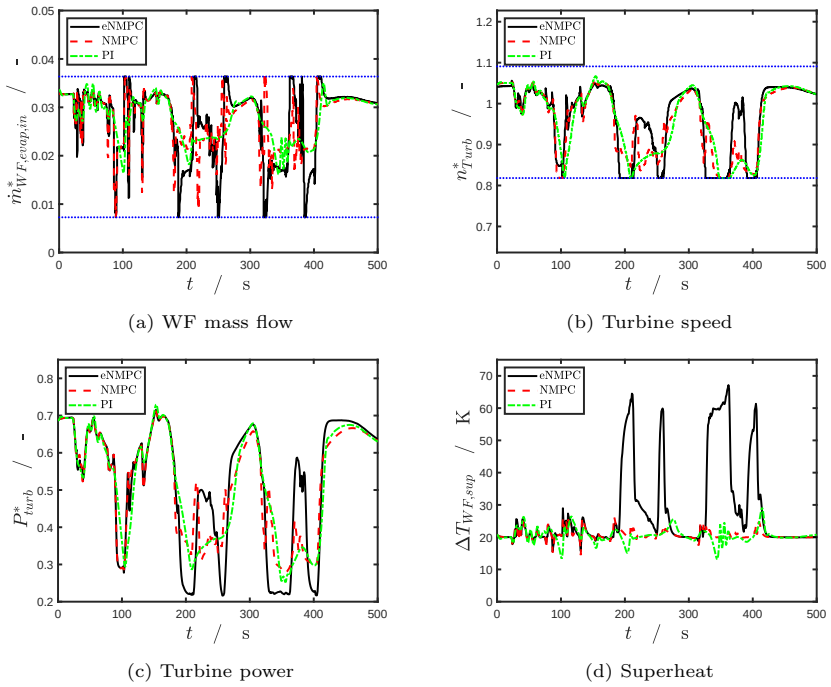

(a) WF mass flow

(b) Turbine speed

(c) Turbine power

(d) Superheat

Figure 7: Results for eNMPC, NMPC and PI-ff. Input constraints are indicated by the blue dotted lines.

can be seen, significant peaks in superheat occur in eNMPC (Fig. 7d). This reflects results found in [38] and similar results can be seen in [50], however, since no disturbance prediction is available, this behavior is surprising. Apparently, the advantages of temporarily operating at increased superheat observed in [38]

can also be leveraged without knowledge of future disturbances. Every new measurement of the disturbance is a step change for the optimizer compared to the previous instant. When we researched the phenomenon for our previous publication [38], we found that superheat peaks are present in the optimal solution for step experiments when the steps in $\dot{m}_{exh}$ are of sufficient duration. In agreement with this observation, the peaks in superheat occur from $t \approx 200\,\mathrm{s}$ on, where the profile for $\dot{m}_{exh}$ is smoother than in earlier periods.

PI-ff is able to track the superheat set-point well and maintains the system above a superheat threshold of $\Delta T_{sup} = 10$ K. The performance is mostly comparable to NMPC which is also able to track the superheat set-point with a maximum deviation of less than 10 K. Since, all controllers stay above this threshold, we do not consider bypassing the turbine herein. However, PI-ff operates below the superheat set-point more often and for more prolonged periods than NMPC. This is mostly in situations where a fast decrease in $\dot{m}_{WF,in}$ is required and the PI controller does not act with the same speed as the idealized model-based controllers (Fig. 7a). In a case where the violation of the superheat constraints results in the turbine being bypassed, these periods would significantly decrease power production. Thus, it is important to find good tuning parameters and to choose sufficient back-off for the superheat set-point. On the other hand, the PI-ff control profile for $\dot{m}_{WF,in}$ (Fig. 7a) is much smoother than for the eNMPC and NMPC. Consequently, operation is less straining for the components and a longer lifetime could be expected.

The separation of the turbine optimization in the tracking NMPC strategy appears to have no detrimental effect on system performance. In fact, notable differences in turbine speed for eNMPC and NMPC (Fig. 7b) only occur in concordance with peaks in eNMPC superheat. Before the first peak occurs (shortly before 200 s), there is no visible difference in turbine power production for eNMPC and NMPC (Fig. 7c).

We assess the examined strategies by comparing average scaled net power $P^*_{net,av}$, presented in Tab. 3.

$$P^*_{net,av} = \frac{\int_{t_0}^{t_f} \left(P^*_{turb}(t) - P^*_{pump}(t) \right) \mathrm{d}t}{t_f^{OCP} - t_0} \tag{11}$$

From the table, we make two main observations. First, splitting the control

	$P^*_{net,av}$
eNMPC	0.516
NMPC	0.514
PI-ff	0.513

Table 3: Average scaled net power for eNMPC, NMPC and PI-ff.

problem in a superheat set-point tracking task and separate turbine optimization yields similar power production to eNMPC while reducing the control problem to a single-input single-output problem. In fact, the losses in power produced are less than 0.5 %. Second, the decoupled problem can be conveniently addressed with a PI controller with marginal performance losses compared to much more complex model-based control. This finding is in agreement with literature where 2 % losses of PI controller compared to eNMPC are reported [28]. The much higher losses associated with a PI controller in [27] and [32] are mostly due to intermediate turbine bypassing when the superheat constraint is violated. This implies that for a PI controller, a set-point with sufficient back-off from the superheat constraint should be chosen as the resulting losses in produced power are moderate compared with the losses of temporarily bypassing the turbine. We found that increasing the superheat set-point by 5 K reduces produced power by about 1 %. Note that in [27] a double heat exchanger system was examined which is harder to control.

Using a prediction of the disturbance in NMPC is proposed in [51]. In case of a perfect disturbance prediction, we find that PI-ff produces roughly 2 % less power than eNMPC and NMPC. Furthermore, the improved NMPC superheat

constraint compliance would allow to reduce the superheat set-point, a result also observed in [51].

Our results imply that NMPC has only small advantages over more traditional control strategies. Due to the specific system topology, the control problem effectively reduces to a SISO problem, thus eliminating potential advantages of a centralized control structure. Furthermore, the economically optimal control policy can be approximated with small losses by tracking minimal superheat. Finally, sufficient back-up can compensate for the slightly poorer tracking performance of a PID-type controller and ensure that the turbine is not bypassed at moderate economic cost.

5. Conclusions and Outlook

Controlling an ORC on board of a vehicle operated in street traffic is a challenging task. The system has to be operated safely and efficiently under highly transient heat source conditions. Control updates have to be made at high frequency and the control algorithm has to be executed on on-board hardware with limited computational resources.

Based on our findings from dynamic optimization [38], we proposed and assessed several control strategies in this work. We compared the performance of a nonlinear model predictive control algorithm (NMPC) and a PI controller with feed-forward term (PI-ff). Furthermore, we discussed how the economic optimal control problem with two DOF can be recast as a single-input single-output tracking control problem and an additional steady-state optimization.

We compared the proposed controllers in a case study containing parts of the WHTC. From the results we deduced two main findings. First, decomposing the control problem into two simpler subproblems results only in small losses with respect to power production. This decomposition reduces the optimal control

problem to a single-input single-output problem which reduces the computational load for model-based algorithms and allows for convenient use of single PI controller. Second, losses from using the PI controller with feed-forward term are small with 0.5 % less energy recovered than with economic NMPC. Even when we assumed perfect disturbance predictions, this values only increased to about 2 %.

These results imply that it is unlikely that a vehicle manufacturer would use NMPC for ORC in a vehicle. It has to be considered that the benefits of NMPC only apply to the amount of fuel saved which optimistic estimates put in the range of 5 % so that the additional overall fuel saving resulting from using NMPC would be in the range of 0.1 %. Our idealized NMPC framework is not real-time capable. Others have achieved real-time capability using fast-update algorithms with ACADO [27] and their own RTI implementation [28], albeit on desktop computers. However, even if real-time capability could be achieved on-board, it is questionable whether the small gains in power production are sufficient to outweigh the advantages of PID control, including small development cost compared to NMPC.

When a decentralized control structure is chosen, designing an overall energy management system [39] is an important task. This system should consider all conceivable conditions (e.g., limited cooling capacity) which could affect ORC operation. In our previous publication [38], we showed that dynamic optimization can be a valuable tool to understand optimal system behavior and draw conclusions on an suitable decentralized control strategies. In this work, we have not considered a scenario where the amount of power that can be utilized is temporarily limited. For this, we would require an energy management system that first reduces power production through manipulation of WF mass flow and turbine speed and switches to a mode where the exhaust bypass valve can be utilized when other constraints (e.g. maximum WF temperature) become active. In future work, this case and further scenarios should be assessed. An

interesting extension would be the consideration of the condenser, which to date has not been adequately addressed in literature. In particular, it would be interesting to assess the effects on the economically optimal operation when a cost for cooling could be quantified (e.g., additional power consumption of radiator fan).

NMPC in applications with limited computational resources, however, remains an important focus of research. Further work could try exploit recent advances in machine learning for NMPC [30, 52] and the combination with fast-update methods [53].

Acknowledgments

The work leading to this contribution was funded by the Federal Ministry for Economic Affairs and Energy (BMWi) according to a resolution passed by the German Federal Parliament under grant number 19U14010C. The authors gratefully acknowledge the financial support of the Kopernikus project SynErgie by the Bundesministerium für Bildung und Forschung (BMBF) and the project supervision by the project management organization Projektträger Jülich (PtJ).

Appendix A. Selected model equations

Here, we present a description of selected model equations, taken from [40], required for understanding the model. For a full description, including parameter values resulting from a dynamic parameter estimation, we refer the reader to [40].

Appendix A.1. Evaporator moving boundary model

For control volumes with single-phase flow, we get the following mass (A.1) and energy (A.2) balances

$$A\left((z_a - z_b)\,\frac{\mathrm{d}\bar{\rho}}{\mathrm{d}t} + \bar{\rho}\,\frac{\mathrm{d}\,(z_b - z_a)}{\mathrm{d}t}\right) + \rho_a A\,\frac{\mathrm{d}z_a}{\mathrm{d}t} - \rho_b A\,\frac{\mathrm{d}z_b}{\mathrm{d}t} = \dot{m}_a - \dot{m}_b, \quad \text{(A.1)}$$

$$A\left(\left(z_b-z_a\right)\bar{\rho}\frac{\mathrm{d}\bar{h}}{\mathrm{d}t}+\left(z_b-z_a\right)\bar{h}\frac{\mathrm{d}\bar{\rho}}{\mathrm{d}t}+\bar{\rho}\bar{h}\frac{\mathrm{d}\left(z_b-z_a\right)}{\mathrm{d}t}\right)-A\left(z_b-z_a\right)\frac{\mathrm{d}p}{\mathrm{d}t}$$
$$+\rho_a h_a A\frac{\mathrm{d}z_a}{\mathrm{d}t}-\rho_b h_b A\frac{\mathrm{d}z_b}{\mathrm{d}t}=\dot{m}_a h_a-\dot{m}_b h_b+b_{WF}\alpha_{WF}\left(z_b-z_a\right)\left(T_w-\bar{T}\right), \tag{A.2}$$

where A is the cross-sectional area of the fluid channel and z is the longitudinal coordinate. ρ, T and $\dot{m}$ are density, temperature and mass flow of the WF, where the subscripts a and b indicate quantities of the left-hand and right-hand boundary of the zones and the overline indicates averaged quantities. t is the time, b_{WF} the width of the fluid channel and α_{WF} is the heat transfer coefficient from WF to the wall. The last term on the right hand side of (A.2) is the heat flow from the wall into the WF. As $\bar{\rho}$ and $\bar{h}$ are algebraic quantities, we account for their time dependence by constructing their total differential w.r.t. the differential quantities (A.3) and (A.4) and inserting them into (A.1) and (A.2), in order to obtain formulations, where only actual differential quantities appear in time derivatives.

$$\frac{\mathrm{d}\bar{\rho}}{\mathrm{d}t}=\frac{\partial\bar{\rho}}{\partial p}\frac{\mathrm{d}p}{\mathrm{d}t}+\frac{\partial\bar{\rho}}{\partial\bar{h}}\frac{\mathrm{d}\bar{h}}{\mathrm{d}t} \tag{A.3}$$

$$\frac{\mathrm{d}\bar{h}}{\mathrm{d}t}=\frac{1}{2}\left(\frac{\mathrm{d}h_a}{\mathrm{d}t}+\frac{\mathrm{d}h_b}{\mathrm{d}t}\right) \tag{A.4}$$

For the two-phase zone, the mass (A.5) and energy (A.6) balances are

$$A\Big(\left(\bar{\gamma}\rho''+\left(1-\bar{\gamma}\right)\rho'\right)\frac{\mathrm{d}\left(z_b-z_a\right)}{\mathrm{d}t}+\left(z_b-z_a\right)\Big(\frac{\mathrm{d}\bar{\gamma}}{\mathrm{d}t}\left(\rho''-\rho'\right)$$
$$+\bar{\gamma}\frac{\partial\rho''}{\partial p}\frac{\mathrm{d}p}{\mathrm{d}t}+\left(1-\bar{\gamma}\right)\frac{\partial\rho'}{\partial p}\frac{\mathrm{d}p}{\mathrm{d}t}\Big)\Big)+\rho_a A\frac{\mathrm{d}z_a}{\mathrm{d}t}-\rho_b A\frac{\mathrm{d}z_b}{\mathrm{d}t}=\dot{m}_a-\dot{m}_b, \tag{A.5}$$

$$
\begin{aligned}
A\Big(\frac{\mathrm{d}\left(z_b - z_a\right)}{\mathrm{d}t}\left(\bar{\gamma}\rho''h'' + \left(1-\bar{\gamma}\right)\rho'h'\right) + \left(z_b - z_a\right)\Big(\frac{\mathrm{d}\bar{\gamma}}{\mathrm{d}t}\left(\rho''h'' - \rho'h'\right) \\
+\bar{\gamma}h''\frac{\mathrm{d}\rho''}{\mathrm{d}p}\frac{\mathrm{d}p}{\mathrm{d}t} + \left(1-\bar{\gamma}\right)h'\frac{\mathrm{d}\rho'}{\mathrm{d}p}\frac{\mathrm{d}p}{\mathrm{d}t} + \bar{\gamma}\rho''\frac{\mathrm{d}h''}{\mathrm{d}p}\frac{\mathrm{d}p}{\mathrm{d}t} + \left(1-\bar{\gamma}\right)\rho'\frac{\mathrm{d}h'}{\mathrm{d}p}\frac{\mathrm{d}p}{\mathrm{d}t}\Big)\Big) \\
-A\left(z_b - z_a\right)\frac{\mathrm{d}p}{\mathrm{d}t} + A\rho_a h_a\frac{\mathrm{d}z_a}{\mathrm{d}t} - A\rho_b h_b\frac{\mathrm{d}z_b}{\mathrm{d}t} \\
= \dot{m}_a h_a - \dot{m}_b h_b + b_{WF}\alpha_{WF}\left(z_b - z_a\right)\left(T_w - \bar{T}\right), \qquad \text{(A.6)}
\end{aligned}
$$

where $\bar{\gamma}$ is the average void fraction calculated with (A.7) and the superscripts $'$ and $''$ indicate quantities at liquid and vapor saturation, respectively. The time derivative of the average void fraction can be expressed by constructing the total differential w.r.t. the differential quantities (A.8).

$$
\begin{aligned}
\bar{\gamma} = \frac{\rho'}{\left(h_0 - h_2\right)\left(\rho' - \rho''\right)^2}\Bigg\{\left(h_0 - h_2\right)\rho' + \rho''\Bigg[h_2 - h_0 \\
+ \left(h' - h''\right)\ln\left(\frac{\rho''\left(h'' - h_0\right)}{\rho'\left(h_2 - h'\right)}\right)\Bigg]\Bigg\} \qquad \text{(A.7)}
\end{aligned}
$$

$$
\frac{\mathrm{d}\bar{\gamma}}{\mathrm{d}t} = \frac{\partial\bar{\gamma}}{\partial h_0}\frac{\mathrm{d}h_0}{\mathrm{d}t} + \frac{\partial\bar{\gamma}}{\partial h_2}\frac{\mathrm{d}h_2}{\mathrm{d}t} + \frac{\partial\bar{\gamma}}{\partial p}\frac{\mathrm{d}p}{\mathrm{d}t} \qquad \text{(A.8)}
$$

The energy balance for each wall zone (A.9) reads,

$$
\begin{aligned}
A_w\rho_w c_{p_w}\left(l_i\frac{\mathrm{d}T_{w_i}}{\mathrm{d}t} + \left(T_{w,B_{i,i-1}} - T_{w_i}\right)\frac{\mathrm{d}z_{a,i}}{\mathrm{d}t} + \left(T_{w_i} - T_{w,B_{i,i+1}}\right)\frac{\mathrm{d}z_{b,i}}{\mathrm{d}t}\right) \\
= \dot{Q}_{exh_i} - b_{WF}\alpha_{WF,i}l_i\left(T_{w_i} - \bar{T}_i\right) - \alpha_{amb}p_{evap}l_i\left(T_{w_i} - T_{amb}\right), \qquad \text{(A.9)}
\end{aligned}
$$

where A_w, ρ_w and c_{p_w} are the wall cross-sectional area, density and heat capacity. T_{w_i} is the temperature of the respective wall zone and $T_{w,B_{i,i-1}}$ and $T_{w,B_{i,i+1}}$ are the wall temperatures at the left- and right-hand boundary of the zone, which are calculated using a length-weighted average, as suggested in [54]. $\dot{Q}_{exh_i}$ is the amount of heat transfered from the exhaust gas to the wall, b_{WF} is the WF channel width and α_i the heat transfer coefficient for the WF in the respective zone. We introduce a term accounting for heat loss from the exchanger wall to the environment, in which α_{amb} is the heat transfer coefficient, p_{evap} the

HX perimeter and T_{amb} the ambient temperature.

By analytical integration of the quasi-stationary energy balance on the exhaust side from interface $i+1$ to interface i assuming static one dimensional flow [55], the temperature at the end of one element can be calculated as in (A.10) and the heat transfered to the wall as in (A.11). Both the exhaust heat capacity c_{p,exh_i} and the heat transfer coefficient α_{exh_i} are assumed constant over one element. $\dot{m}_{exh}$, T_{exh} and b_{exh} are mass flow, temperature and width of the exhaust channel.

$$T_{exh_i} = T_{w_i} + \left(T_{exh_{i+1}} - T_{w_i}\right) \exp\left(-\frac{\alpha_{exh_i} b_{exh}}{\dot{m}_{exh} c_{p,exh_i}} l_i\right), \quad i \in [0,2] \tag{A.10}$$

$$\dot{Q}_{exh_i} = \dot{m}_{exh} c_{p,exh_i} \left(T_{exh_{i+1}} - T_{exh_i}\right) \tag{A.11}$$

Appendix A.2. Pump and turbine models

We model the pump assuming a fixed isentropic and mechanical efficiency ($\eta_{is,pump}$, $\eta_{mech,pump}$), according to (A.12). Within the model, we set both efficiencies to 0.9.

$$P_{pump} = \frac{1}{\eta_{mech,pump}} \cdot \dot{m}_{WF} \cdot \frac{h_{out,is} - h_{in}}{\eta_{is,pump}} \tag{A.12}$$

For the turbine, we use (A.13) to calculate the power output P_{turb}.

$$P_{turb} = \eta_{mech,turb} \cdot \dot{m}_{WF} \cdot \eta_{is,turb} \cdot (h_{in} - h_{out,is}) \tag{A.13}$$

The isentropic efficiency is a function of pressure ratio between high and low pressure and turbine speed. For this, we choose a polynomial function of third order with respect to pressure ratio and fifth order with respect to turbine speed. The mechanical efficiency, in contrast, is a function of turbine speed n (second order polynomial) and torque M (fifth order polynomial).

References

[1] C. Sprouse, III, C. Depcik, Review of organic Rankine cycles for internal combustion engine exhaust waste heat recovery, Applied Thermal Engineering 51 (1–2) (2013) 711–722.

[2] A. T. Hoang, Waste heat recovery from diesel engines based on organic rankine cycle, Applied Energy 231 (2018) 138–166. doi:10.1016/j.apenergy.2018.09.022.

[3] R. Pili, A. Romagnoli, K. Kamossa, A. Schuster, H. Spliethoff, C. Wieland, Organic rankine cycles (ORC) for mobile applications – economic feasibility in different transportation sectors, Applied Energy 204 (2017) 1188–1197. doi:10.1016/j.apenergy.2017.04.056.

[4] T. Endo, S. Kawajiri, Y. Kojima, K. Takahashi, T. Baba, S. Ibaraki, T. Takahashi, M. Shinohara, Study on maximizing exergy in automotive engines, in: SAE Technical Paper Series, SAE International, 2007. doi:10.4271/2007-01-0257.

[5] A. Boretti, Recovery of exhaust and coolant heat with R245fa organic Rankine cycles in a hybrid passenger car with a naturally aspirated gasoline engine, Applied Thermal Engineering 36 (2012) 73–77. doi:10.1016/j.applthermaleng.2011.11.060.
URL http://www.sciencedirect.com/science/article/pii/S1359431111006880

[6] T. A. Horst, H.-S. Rottengruber, M. Seifert, J. Ringler, Dynamic heat exchanger model for performance prediction and control system design of automotive waste heat recovery systems, Applied Energy 105 (2013) 293–303.

[7] T. A. Horst, W. Tegethoff, P. Eilts, J. Koehler, Prediction of dynamic Rankine Cycle waste heat recovery performance and fuel saving potential in passenger car applications considering interactions with vehicles' energy

management, Energy Conversion and Management 78 (2014) 438–451. doi:10.1016/j.enconman.2013.10.074.
URL http://www.sciencedirect.com/science/article/pii/S0196890413007097

[8] J. Fu, J. Liu, R. Feng, Y. Yang, L. Wang, Y. Wang, Energy and exergy analysis on gasoline engine based on mapping characteristics experiment, Applied Energy 102 (2013) 622–630. doi:10.1016/j.apenergy.2012.08.013.

[9] S. Quoilin, S. Declaye, B. F. Tchanche, V. Lemort, Thermo-economic optimization of waste heat recovery Organic Rankine Cycles, Applied Thermal Engineering 31 (14–15) (2011) 2885–2893. doi:10.1016/j.applthermaleng.2011.05.014.
URL http://www.sciencedirect.com/science/article/pii/S1359431111002663

[10] Y. Dai, J. Wang, L. Gao, Parametric optimization and comparative study of organic Rankine cycle (ORC) for low grade waste heat recovery, Energy Conversion and Management 50 (3) (2009) 576–582. doi:10.1016/j.enconman.2008.10.018.
URL http://www.sciencedirect.com/science/article/pii/S0196890408004342

[11] A. M. Schweidtmann, W. R. Huster, J. T. Lüthje, A. Mitsos, Deterministic global process optimization: Accurate (single-species) properties via artificial neural networks, Computers & Chemical Engineering 121 (2019) 67–74. doi:10.1016/j.compchemeng.2018.10.007.

[12] J. Schilling, K. Eichler, B. Kölsch, S. Pischinger, A. Bardow, Integrated design of working fluid and organic rankine cycle utilizing transient exhaust gases of heavy-duty vehicles, Applied Energy 255 (2019) 113207. doi:10.1016/j.apenergy.2019.05.010.

[13] D. Tillmanns, J. Petzschmann, J. Schilling, C. Gertig, A. Bardow, ORC on tour: Integrated design of dynamic ORC processes and working fluids for waste-heat recovery from heavy-duty vehicles, in: Computer Aided Chemical Engineering, Elsevier, 2019, pp. 163–168. doi:10.1016/b978-0-12-818634-3.50028-x.

[14] B. Xu, D. Rathod, A. Yebi, Z. Filipi, S. Onori, M. Hoffman, A comprehensive review of organic rankine cycle waste heat recovery systems in heavy-duty diesel engine applications, Renewable and Sustainable Energy Reviews 107 (2019) 145–170. doi:10.1016/j.rser.2019.03.012.

[15] D. Jolevski, O. Bego, P. Sarajcev, Control structure design and dynamics modelling of the organic Rankine cycle system, Energy 121 (2017) 193–204.

[16] S. Quoilin, R. Aumann, A. Grill, A. Schuster, V. Lemort, H. Spliethoff, Dynamic modeling and optimal control strategy of waste heat recovery Organic Rankine Cycles, Applied Energy 88 (6) (2011) 2183–2190.

[17] V. Grelet, P. Dufour, M. Nadri, T. Reiche, V. Lemort, Modeling and control of rankine based waste heat recovery systems for heavy duty trucks, IFAC-PapersOnLine 48 (8) (2015) 568–573. doi:10.1016/j.ifacol.2015.09.028.

[18] A. Hernandez, A. Desideri, C. Ionescu, S. Quoilin, V. Lemort, R. de Keyser, Increasing the eciency of Organic Rankine Cycle Technology by means of Multivariable Predictive Control, The International Federation of Automatic Control, Cape Town, South Africa. August 24-29, 2014 (2014).

[19] J. Zhang, Y. Zhou, R. Wang, J. Xu, F. Fang, Modeling and constrained multivariable predictive control for ORC (Organic Rankine Cycle) based waste heat energy conversion systems, Energy 66 (2014) 128–138.

[20] E. Feru, F. Willems, B. de Jager, M. Steinbuch, Modeling and Control of a Parallel Waste Heat Recovery System for Euro-VI Heavy-Duty Diesel Engines, Energies 7 (10) (2014) 6571–6592. doi:10.3390/en7106571.

[21] H. Koppauer, W. Kemmetmüller, A. Kugi, Model predictive control of an automotive waste heat recovery system, Control Engineering Practice 81 (2018) 28–42. doi:10.1016/j.conengprac.2018.09.005.

[22] J. Peralez, P. Tona, M. Nadri, P. Dufour, A. Sciarretta, Optimal control for an organic rankine cycle on board a diesel-electric railcar, Journal of Process Control 33 (2015) 1–13.

[23] A. Yebi, B. Xu, X. Liu, J. Shutty, P. Anschel, S. Onori, Z. Filipi, M. Hoffman, Nonlinear model predictive control strategies for a parallel evaporator diesel engine waste heat recovery system, in: ASME 2016 Dynamic Systems and Control Conference, American Society of Mechanical Engineers, 2016. doi:10.1115/dscc2016-9801.

[24] M. Crialesi Esposito, N. Pompini, A. Gambarotta, V. Chandrasekaran, J. Zhou, M. Canova, Nonlinear Model Predictive Control of an Organic Rankine Cycle for Exhaust Waste Heat Recovery in Automotive Engines, IFAC-PapersOnLine 48 (15) (2015) 411–418.

[25] P. Petr, C. Schröder, J. Köhler, M. Gräber, Optimal Control of Waste Heat Recovery Systems Applying Nonlinear Model Predictive Control, in: V. Lemort, S. Quoilin, M. de Paepe, M. van den Broek (Eds.), Proceedings of the 3rd International Seminar on ORC Power Systems, 2015, pp. 1183–1192.

[26] M. Ellis, H. Durand, P. D. Christofides, A tutorial review of economic model predictive control methods, Journal of Process Control 24 (8) (2014) 1156–1178. doi:10.1016/j.jprocont.2014.03.010.

[27] A. Yebi, B. Xu, X. Liu, J. Shutty, P. Anschel, Z. Filipi, S. Onori, M. Hoffman, Estimation and Predictive Control of a Parallel Evaporator Diesel Engine Waste Heat Recovery System, IEEE Transactions on Control Systems Technology (2017) 1–14.

[28] E. Guerrero Merino, J. P. Schloder, C. Kirches, A nonlinear model-predictive control scheme for a heavy duty truck's waste heat recovery system featuring moving horizon estimation, in: 2018 Annual American Control Conference (ACC), IEEE, 2018. doi:10.23919/acc.2018.8431307.

[29] I. J. Wolf, W. Marquardt, Fast NMPC schemes for regulatory and economic NMPC – a review, Journal of Process Control 44 (2016) 162–183. doi:10.1016/j.jprocont.2016.05.002.

[30] Y. Vaupel, A. Caspari, N. C. Hamacher, W. R. Huster, A. Mhamdi, I. G. Kevrekidis, A. Mitsos, Artificial neural networks for real-time model predictive control of organic rankine cycles for waste heat recovery, in: S. Karellas, E. Kakaras (Eds.), Proceedings of the 5th International Seminar on ORC Power Systems, 2019.

[31] V. Grelet, P. Dufour, M. Nadri, V. Lemort, T. Reiche, Explicit multi-model predictive control of a waste heat rankine based system for heavy duty trucks, in: 2015 54th IEEE Conference on Decision and Control (CDC), IEEE, 2015. doi:10.1109/cdc.2015.7402105.

[32] B. Xu, D. Rathod, A. Yebi, Z. Filipi, A comparative analysis of real-time power optimization for organic rankine cycle waste heat recovery systems, Applied Thermal Engineering 164 (2020) 114442. doi:10.1016/j.applthermaleng.2019.114442.

[33] M. Diehl, H. G. Bock, J. P. Schlöder, A real-time iteration scheme for nonlinear optimization in optimal feedback control, SIAM Journal on Control and Optimization 43 (5) (2005) 1714–1736. doi:10.1137/s0363012902400713.

[34] B. Houska, H. J. Ferreau, M. Diehl, ACADO toolkit-an open-source framework for automatic control and dynamic optimization, Optimal Control Applications and Methods 32 (3) (2011) 298–312. doi:10.1002/oca.939.

[35] P. Tona, J. Peralez, Control of Organic Rankine Cycle Systems on board Heavy-Duty Vehicles: a Survey, IFAC-PapersOnLine 48 (15) (2015) 419–426. doi:10.1016/j.ifacol.2015.10.060.

[36] J. Peralez, M. Nadri, P. Dufour, P. Tona, A. Sciarretta, Organic Rankine Cycle for Vehicles: Control Design and Experimental Results, IEEE Transactions on Control Systems Technology (2016) 1–14doi:10.1109/TCST.2016.2574760.

[37] B. Xu, A. Yebi, S. Onori, Z. Filipi, X. Liu, J. Shutty, P. Anschel, M. Hoffman, Transient power optimization of an organic rankine cycle waste heat recovery system for heavy-duty diesel engine applications, SAE International Journal of Alternative Powertrains 6 (1) (Mar. 2017). doi:10.4271/2017-01-0133.

[38] Y. Vaupel, W. R. Huster, A. Mhamdi, A. Mitsos, Optimal operating policies for organic rankine cycles for waste recovery under transient conditions, Submitted (05 March 2020).

[39] F. Willems, F. Kupper, G. Rascanu, E. Feru, Integrated Energy and Emission Management for Diesel Engines with Waste Heat Recovery Using Dynamic Models, Oil & Gas Science and Technology – Revue d'IFP Energies nouvelles 70 (1) (2015) 143–158. doi:10.2516/ogst/2013210.

[40] W. R. Huster, Y. Vaupel, A. Mhamdi, A. Mitsos, Validated dynamic model of an organic Rankine cycle (ORC) for waste heat recovery in a diesel truck, Energy 151 (2018) 647–661.

[41] J. M. Jensen, Dynamic modeling of thermo-fluid systems: With focus on evaporators for refrigeration, Vol. 2003-01 of MEK-ET-PHD, Department of Mechanical Engineering, Technical University of Denmark, Lyngby, 2003.

[42] Y. Vaupel, W. R. Huster, F. Holtorf, A. Mhamdi, A. Mitsos, Analysis and improvement of dynamic heat exchanger models for nominal and start-up

operation, Energy 169 (2019) 1191–1201. doi:10.1016/j.energy.2018.12.048.

[43] V. Lemort, A. Legros, Positive displacement expanders for organic rankine cycle systems, in: Organic Rankine Cycle (ORC) Power Systems, Elsevier, 2017, pp. 361–396. doi:10.1016/b978-0-08-100510-1.00012-0.

[44] A. Caspari, A. Bremen, J. Faust, F. Jung, C. Kappatou, S. Sass, Y. Vaupel, R. Hannemann-Tamás, A. Mhamdi, A. Mitsos, DyOS - a framework for optimization of large-scale differential algebraic equation systems, in: Computer Aided Chemical Engineering, Elsevier, 2019, pp. 619–624. doi:10.1016/b978-0-12-818634-3.50104-1.

[45] R. Hannemann, W. Marquardt, U. Naumann, B. Gendler, Discrete first- and second-order adjoints and automatic differentiation for the sensitivity analysis of dynamic models, Procedia Computer Science 1 (1) (2010) 297–305. doi:10.1016/j.procs.2010.04.033.

[46] P. E. Gill, W. Murray, M. A. Saunders, SNOPT: An SQP algorithm for large-scale constrained optimization, SIAM Review 47 (1) (2005) 99–131. doi:10.1137/s0036144504446096.

[47] N. M. C. de Oliveira, L. T. Biegler, Constraint handing and stability properties of model-predictive control, AIChE Journal 40 (7) (1994) 1138–1155. doi:10.1002/aic.690400706.

[48] S. Skogestad, I. Postlethwaite, Multivariable feedback control: Analysis and design, 2nd Edition, Wiley, Chichester, 2010.

[49] L. Grüne, J. Pannek, Nonlinear Model Predictive Control, Springer International Publishing, 2017. doi:10.1007/978-3-319-46024-6.

[50] E. E. Guerrero Merino, Real-time optimization for estimation and control: Application to waste heat recovery for heavy duty trucks, Ph.D. thesis, University of Heidelberg (2018).

[51] D. Rathod, B. Xu, A. Yebi, A. Vahidi, Z. Filipi, M. Hoffman, A look-ahead model predictive optimal control strategy of a waste heat recovery-organic rankine cycle for automotive application, in: SAE Technical Paper Series, SAE International, 2019. doi:10.4271/2019-01-1130.

[52] S. Lucia, B. Karg, A deep learning-based approach to robust nonlinear model predictive control, IFAC-PapersOnLine 51 (20) (2018) 511–516. doi:10.1016/j.ifacol.2018.11.038.

[53] Y. Vaupel, N. C. Hamacher, A. Caspari, A. Mhamdi, I. G. Kevrekidis, A. Mitsos, Accelerating nonlinear model predictive control through machine learning, Journal of Process Control 92 (2020) 261–270. doi:10.1016/j.jprocont.2020.06.012.

[54] W.-J. Zhang, C.-L. Zhang, A generalized moving-boundary model for transient simulation of dry-expansion evaporators under larger disturbances, International Journal of Refrigeration 29 (7) (2006) 1119–1127.

[55] T. L. McKinley, A. G. Alleyne, An advanced nonlinear switched heat exchanger model for vapor compression cycles using the moving-boundary method, International Journal of Refrigeration 31 (7) (2008) 1253–1264.